

## On the $B \leftarrow X$ transitions of expansion cooled silver halides

Guido J. Stueber, Martin Foltin, and Elliot R. Bernstein

Citation: *The Journal of Chemical Physics* **109**, 9831 (1998); doi: 10.1063/1.477652

View online: <http://dx.doi.org/10.1063/1.477652>

View Table of Contents: <http://aip.scitation.org/toc/jcp/109/22>

Published by the [American Institute of Physics](#)

---

---

**COMPLETELY**

**REDESIGNED!**



**PHYSICS  
TODAY**

*Physics Today* Buyer's Guide  
Search with a purpose.

# On the $B \leftarrow X$ transitions of expansion cooled silver halides

Guido J. Stueber, Martin Foltin, and Elliot R. Bernstein<sup>a)</sup>

*Department of Chemistry, Colorado State University, Fort Collins, Colorado 80523-1872*

(Received 16 July 1998; accepted 1 September 1998)

Fluorescence excitation and mass-resolved excitation spectroscopy of jet-cooled silver halide ( $\text{AgX}$ ) bare molecules are explored for the  $B \leftarrow X$  systems of  $\text{AgCl}$ ,  $\text{AgBr}$ , and  $\text{AgI}$ . These spectra are compared to those from static gas measurements. The continuous-wave expansion molecular beam of  $\text{Ar-He}$  with  $\text{AgX}$  species is generated at a temperature of  $1100^\circ\text{C}$ . For  $\text{AgI}$  two types of progressions are shown to appear in  $31\,000\text{--}33\,000\text{ cm}^{-1}$  range. The first set of transitions is attributed to the  $B$  state and is quite similar to the other  $\text{AgX}$  molecule's  $B \leftarrow X$  transitions. The second set has been previously observed for high-temperature  $\text{AgI}$  vapor as a partly resolved series of features on a broad absorption. The nature of this state and whether it arises from a level crossing between the  $B$  surface and an unobserved state is not clear. We analyze two different possible explanations for the newly resolved  $B'$  progression: The  $B$  and  $B'$  progressions involve two different excited electronic states; and both progressions belong to one excited electronic state with a complicated single adiabatic potential surface. Computation of vibrational harmonic and anharmonic constants suggests that the potential shape of the  $B/B'$  state is substantially different from that of a common anharmonic oscillator. The nature of the  $B/B'$  surface must be resolved through detailed and accurate *ab initio* calculations.  $\text{Ag}$  ions produced by  $1+2$  photoionization of  $\text{AgX}$  at longer wavelengths are not fragmentation products of  $\text{AgX}$  ions, but rather arise from the dissociation of a neutral  $\text{AgX}$  in a highly excited state. This intermediate state at  $\sim 62\,000\text{ cm}^{-1}$  is accessed from the  $B$  state by absorption of a photon of approximately the same energy as required for the  $B \leftarrow X$   $\text{AgX}$  transition. © 1998 American Institute of Physics. [S0021-9606(98)00946-5]

## I. INTRODUCTION

The spectroscopy and photophysics of silver halide crystals is a broad subject with a vast literature.<sup>1-3</sup> Because of the practical importance of the silver halides in photography, much of the literature is relevant to the photophysics of latent image formation. The electronic spectroscopy of the  $B \leftarrow X$  transition of silver halide molecules ( $\text{AgX}$ ,  $\text{X}=\text{F}$ ,  $\text{Cl}$ ,  $\text{Br}$ ,  $\text{I}$ ) in the vapor phase was initially studied in the 1930s, later in the 1960s, and led to quite reliable characterization of the respective potential curves.<sup>4-8</sup> This insight was achieved by fitting mostly "hot" transitions arising from higher vibrational levels of the ground state and populating only very few vibrational levels of the  $B$  state. Brice reported for  $\text{AgI}$  the appearance of additional weak peaks on top of a broad absorption between  $31\,670$  and  $33\,150\text{ cm}^{-1}$ , but a conclusive assignment for these features was not offered.<sup>9</sup>

No modern molecular jet spectroscopic studies have been reported for these molecules; however, Wang and Gole<sup>10</sup> have reported the results of a silver vapor-fluorine reaction system for which  $\text{AgF}$  spectra are observed. This study yields fundamental insight into the other silver halide molecules. The assignment of spectral features has been refined by extensive *ab initio* calculations for  $\text{AgF}$ .<sup>11</sup> The first three excited states of  $\text{AgF}$  are labeled  $a\text{O}^-$ ,  $A'1$  (two fine structure components of the  $^3\Sigma^+$  state) and  $\text{AO}^+$  (the single fine structure component of the  $^1\Sigma^+$  state). These excited states are strong mixtures of ionic  $\text{Ag}^+$  ( $^3,^1D;4d^95s^1$ )

$\text{F}^-$  ( $^1S;2s^22p^6$ ) and neutral  $\text{Ag}$  ( $^2S;4d^{10}5s^1$ )  $\text{F}(^2P;2s^22p^5)$  configurations. Avoided crossing of the ionic (bonding) configuration and the neutral (dissociative) configuration occurs near the minima of these surfaces. The resulting mixed adiabatic surfaces are quite complex. These two surfaces dissociate to  $\text{Ag}(^2S)+\text{F}(^2P)$ . The  $\text{BO}^+$  state is the fourth excited state of  $\text{AgF}$  and its assignment is not certain: It can arise from either one of the  $\text{Ag}^+(4d^95s^1)+\text{F}^-(2s^22p^6)$  valence asymptotic ionic fragments or the lowest singlet Rydberg state of the  $\text{Ag}^+(4d^95p)+\text{F}^-(2s^22p^6)$  configuration. Mixing between neutral and ionic configurations of  $\text{AgF}$  is critically dependent on the relative energies of the  $\text{Ag }4d$  and  $\text{F }2p$  levels. Thus, the extent and nature of different configurational mixing in  $\text{AgX}$ ,  $\text{X}=\text{Cl}$ ,  $\text{Br}$ ,  $\text{I}$ , excited states in general may be different for each species.

Despite the outstanding importance of silver halide photochemistry and photophysics for practical applications, surprisingly little information exists on the silver halide molecules or small clusters. We focus our interest in this report on the re-examination of  $\text{AgX}$  spectroscopic characteristics for the  $B \leftarrow X$  transition employing both fluorescence excitation and mass resolved excitation spectroscopies.

## II. EXPERIMENTAL PROCEDURES

The experimental setup and procedures for fluorescence spectroscopy and time-of-flight mass spectroscopy of the supersonic expansion cooled samples are in principle identical

<sup>a)</sup>Electronic mail: erb@lamar.colostate.edu

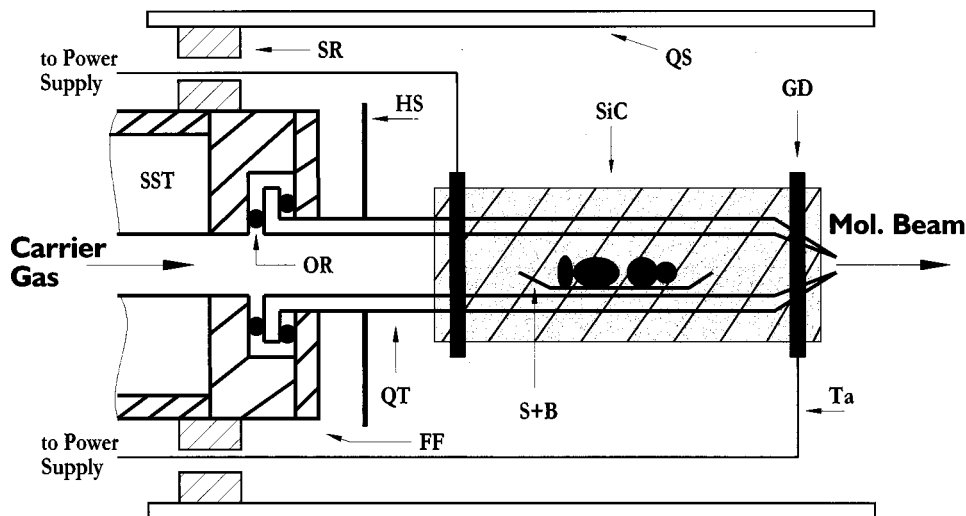


FIG. 1. Schematic drawing of the high-temperature cw nozzle consisting of the principal parts slip-ring (SR), quartz sleeve (QS), power supply (PS), front flange (FF), heat shield (HS), silicon carbide tube heater (SiC), graphite disk (GD), stainless steel tube (SST), O-ring (OR), quartz tube (QT), sample in quartz boat (S+B), and tantalum wire (Ta). This setup enables the sample temperature to be varied between 25 and 1600 °C.

to those described in previous papers<sup>12,13</sup> and will be summarized only briefly here: Variations from these procedures are given below.

The molecular beam is generated thermally by heating the solid silver halide in a continuous-wave (cw) high-temperature quartz nozzle. Figure 1 depicts a schematic drawing of this home built nozzle. The nozzle consists of a 2 in. o.d. stainless steel tube (SST) adjustably mounted on a 9 in. o.d. stainless steel flange (MDC). The quartz nozzle is made from commercial 10 mm i.d., 12.5 mm o.d. tube (QT) by highly precisely pulling one end to a point and cutting the tip to reach the desired orifice diameter. The tube's other end is flared in a right angle flange which is sealed to the stainless steel flange via a Viton-7 O-ring (OR). A second O-ring is used on the nonsealing side of the quartz flange to ensure a moderate and even pressure upon tightening the front retaining flange (FF) to hold the quartz nozzle tube in place. Heat shields (HS) cut from  $\text{Al}_2\text{O}_3$  plates are slip fit on the nozzle tube in order to reduce heat radiation exposure of the metal parts and O-rings.

Useful tip hole diameters are found to be 0.1–0.55 mm. We record, depending on the experimental conditions, vibrationally hot or cold [full width at half maximum (FWHM) about  $5\text{ cm}^{-1}$ ] spectra by choosing appropriate combinations of nozzle tip hole diameter, backing pressure, and sample temperature.

A 75 mm long silicon carbide tube (Hexoloy SA, The Carborundum Company, Niagara Falls, NY) 13 mm i.d., 19 mm o.d., is slip fit to the quartz tube and is used as the heating element (SiC). The actual heater position is such that the nozzle tip is fully covered without interfering with the expanding molecular beam. Two graphite disks (GD) machined from a 33 mm diam rod (EDM Supplies, Downey, CA) are attached to the heater o.d. and two clamps machined of tantalum are employed to provide electrical connection to the power feed-through and eventually to the electrical circuit power supply (PS) outside the chamber.

Since silicon carbide's electrical resistance decreases with increasing temperature, it becomes necessary to control and limit the actual current in the heater power supply circuit. The heater is, therefore, in series with six parallel wired

300 W light bulbs. A typical operating condition is 6 A and 90 V (540 W) across the SiC tube generating a sample temperature of about 1100 °C.

The solid sample (S) is placed in a quartz boat that reaches inside the part of the quartz tube that is completely covered by the heating element. In some cases a quartz sleeve (QS), covered with freshly deposited magnesium oxide on its inner surface, is mounted on an aluminum slip ring (SR) and used as additional radiation shielding. This setup allows an increase of the sample temperature by about 100 °C. The obtained vapor pressures for AgX are given in the literature: 100 Torr at 1297 °C for  $\text{AgCl}$ ,<sup>14</sup> 76.6 Torr at 1200 °C for  $\text{AgBr}$ ,<sup>15</sup> and 93.75 Torr at 1200 °C for  $\text{AgI}$ .<sup>16</sup> The usable range of this high-temperature nozzle is limited to below the softening point of quartz glass, which appears to be about 1650 °C. All supersonic expansions are carried out with ~30 psig of argon, helium, or a 10% Ar–He mixture as carrier gas.

The excitation laser beam generated by a Nd/YAG pumped dye laser crosses the molecular beam at a distance of 10 mm from the nozzle tip for fluorescence excitation experiments. The dye solution for excitation is DCM in methanol; the dye laser output frequency is doubled. Fluorescence is collected and focused directly onto the photocathode of a Hamamatsu R943-02 photomultiplier tube (PMT). In order to prevent scattered laser light from reaching the PMT, several glass filters (HOYA B-370 or B-380), in addition to a stainless steel cone that matches the  $f$ -number of the collection lens, are placed in front of the PMT. The obtained signal-to-noise ratio is about 20:1 in most cases. A gated integrator/boxcar averager (SRS 280) and a personal computer process the PMT output signal.

For mass resolved excitation spectra the focused beam of a 193 nm ArF excimer laser (Lambda Physik) serves as an ionization source. The excimer laser energy is 68–150 mJ per pulse, but only a small fraction of this energy (3–7 mJ) reaches the ionization source due to beam attenuation on the optics and the beam collimation. Both lasers are temporally and spatially overlapped. In some instances the excimer laser is replaced by a second Nd/YAG pumped dye laser operating with fluorescein 548 in methanol–NaOH or DCM in metha-

nol. The ionization laser output is doubled (DCM) or doubled and mixed (F548) with Nd/YAG 1.064  $\mu\text{m}$  radiation to generate the appropriate laser wavelength.

The given experimental setup does not allow the cw nozzle to be directly inserted into the mass spectroscopy vacuum chamber due to final pressure constraints ( $p < 10^{-5}$  Torr) for the mass spectrometer. Hence the fluorescence and mass chambers are connected via a 1 mm orifice nickel skimmer of hyperbolic shape (model MIT-85-1, Beam Dynamics, Inc., Minneapolis, MN). The nozzle tip is placed about 20 mm in front of the skimmer. The molecular beam is generated in the fluorescence chamber and its coldest part passes through the skimmer into the mass chamber where the species are ionized and accelerated up the flight tube of a Wiley–McLaren-type time-of-flight mass spectrometer toward the detector [Galileo Electro-Optics multichannel plate (MCP)]. The skimmer-to-ionization region distance is 15 cm and the length of the ion drift region to the MCP is 1.5 m. Mass spectra are recorded with a digital oscilloscope (Tektronix RTD 720A) and monitored with software described in detail elsewhere.<sup>12</sup>

AgCl, AgBr, and AgI are obtained in their highest available purity grade from Aldrich (Milwaukee, WI) and used without additional purification.

### III. EXPERIMENTAL RESULTS AND DISCUSSION

#### A. Generation and analysis of data

In this paper, we present the results of a study of the  $B \leftarrow X$  transitions of silver halide molecules AgX (X=Cl, Br, I) using three different experimental procedures: Fluorescence excitation (FE) spectroscopy, mass resolved excitation spectroscopy (MRES), and time-of-flight mass spectroscopy (TOFMS). The  $B$  potential surface of AgX is accessible from the  $X$  surface between  $\sim 30\,200$  and  $32\,500\text{ cm}^{-1}$  and is easily accessed by one-photon absorption and detected by FE.

Generally speaking, our findings are consistent with previously reported data on spectroscopy of silver halide vapors in the region  $30\,250$  and  $31\,600\text{ cm}^{-1}$ .<sup>4,6-8</sup> By using our high-temperature cw nozzle and appropriate expansion conditions, we record spectra (FWHM  $\sim 5\text{ cm}^{-1}$ ) arising almost only from the  $X$  state zero-point vibrational level. We adjust the conditions with suitable combinations of nozzle tip hole diameters (0.10–0.55 mm), backing pressures (up to 30 psig of Ar or He) and sample temperatures (from AgX's melting point to  $\sim 1200\text{ }^\circ\text{C}$ ). This allows the detection of spectra with almost no transitions visible from other than the ground-state vibrational level, whereas those experiments on AgX in a heated quartz cell lead to hot spectra with transitions from ground-state levels up to 17. Expansion cooled samples show somewhat broadened peaks with shoulders or even split peaks as a direct consequence of the presence of the various isotopes. In order to clarify this issue we perform experiments using TOFMS and MRES. Both methods require the generation of  $\text{AgX}^+$  ions, which are achieved via a two-color two-photon process. The first photon excites the silver halide molecules to their  $B$  states and the subsequent ionization is accomplished with an excimer laser photon.

The actual time-of-flight mass spectra of AgCl, AgBr, and AgI and their clusters and fragments are reported and discussed in a subsequent paper. We describe in the context of this paper only those parts of the mass spectrometric details that lead to a deeper understanding of the presented FE data. This two-color process results in a triplet mass peak for the AgCl and AgBr bare ions and a doublet for AgI due to the X and Ag isotopes. The MRES for each separate molecular isotopic species can be resolved and separately recorded.

Commonly, the energy of the vibronic transitions of a nonrotating diatomic molecule is given by an expansion in the symbols  $\nu_e$ ,  $\omega_e$ ,  $\omega_e x_e$ ,  $\omega_e y_e$ , and  $\omega_e z_e$ . These fitting parameters have their usual meanings as system origin, vibrational frequency, and anharmonicities<sup>17</sup>

$$\nu = \nu_e + \beta \omega'_e u' - \beta^2 \omega'_e x'_e u'^2 + \beta^3 \omega'_e y'_e u'^3 + \beta^4 \omega'_e z'_e u'^4 - \beta \omega''_e u'' + \beta^2 \omega''_e x''_e u''^2, \quad (1)$$

$$u = (v + \frac{1}{2}) \quad \text{with } v = 0, 1, 2, \dots, \quad (2)$$

$$\beta = \sqrt{\mu/\mu_1}, \quad (3)$$

in which  $\mu$  = reduced mass of the identified “normal” molecule and  $\mu_1$  = reduced mass of the identified “isotopic” molecule. Symbols marked with a prime refer to the excited state, and those marked with a double prime refer to the ground state. We perform a simple least-squares fit of the experimentally observed peak positions to Eq. (1) in order to characterize the potential curves including the vibrational isotope effects.

#### B. Silver chloride

Figure 2 shows the FE spectrum of the  $B \leftarrow X$  transition of AgCl cooled in a supersonic expansion. In some cases the band heads appear to be split due to the vibrational isotope effects of chlorine (<sup>35</sup>Cl and <sup>37</sup>Cl) and silver (<sup>107</sup>Ag and <sup>109</sup>Ag): The FE spectra are thus composed of individual contributions of the abundant isotopes. The actual peak positions for a given AgCl isotope in particular are difficult to extract when the vibrational isotope effect is less than a wave number. Hence much more detailed data are generated from the mass-resolved excitation spectra. Figure 3 pictures the mass resolved excitation spectra of two silver chloride isotopes as well as the spectrum recorded in the corresponding <sup>107</sup>Ag mass channel. The isotopically resolved spectra recorded in the <sup>107</sup>Ag and <sup>109</sup>Ag mass channels reflect directly the  $B \leftarrow X$  transitions of the corresponding <sup>107</sup>Ag and <sup>109</sup>Ag containing AgCl molecules: in particular, <sup>107</sup>Ag <sup>35,37</sup>Cl at  $31\,573.7\text{ cm}^{-1}$  (0,0),  $31\,842.4\text{ cm}^{-1}$  and  $31\,835.2\text{ cm}^{-1}$  (1,0), and  $32\,097.5\text{ cm}^{-1}$  and  $32\,089.3\text{ cm}^{-1}$  (2,0) and <sup>109</sup>Ag <sup>35,37</sup>Cl at  $31\,573.6\text{ cm}^{-1}$  (0,0),  $31\,842.6\text{ cm}^{-1}$  and  $31\,835.3\text{ cm}^{-1}$  (1,0), and  $32\,097.4\text{ cm}^{-1}$  and  $32\,087.8\text{ cm}^{-1}$  (2,0). In this way we also gain information about species that are indistinguishable by MRES due to their identical masses. All observed peak positions recorded in the AgCl mass channels are listed in Table I.

The AgCl (0,0) transition appears as the strongest signal in the FE spectrum in agreement with the fact that the internuclear distance is very similar in the ground and  $B$  state. Mass-resolved excitation spectra for the three silver chloride

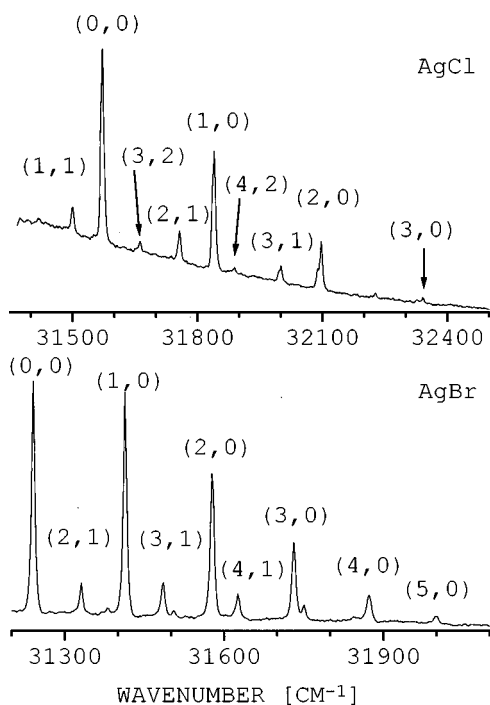


FIG. 2. FE spectra of the  $B \leftarrow X$  transition of expansion cooled AgCl and AgBr. The spectra were taken with a 0.25 mm orifice nozzle, a sample temperature of 1100 °C and a backing pressure of 30 psig He.

mass peaks are very similar to those obtained by fluorescence excitation spectroscopy regarding peak intensities and peak width. The presence of the different silver and chlorine isotopes becomes immediately apparent if one compares individual transitions for the three AgCl mass-resolved data sets, although it is not possible to distinguish between the two species  $^{107}\text{Ag}^{37}\text{Cl}$  and  $^{109}\text{Ag}^{35}\text{Cl}$ . Since the isotopic shift for higher transitions is considerably larger [see Eq. (1)], we assume the observed FE peak positions for the lightest and heaviest AgCl isotopes are of sufficient accuracy to be considered for computing of vibrational constants.

The vibrational analysis based on data given in Table I predicts shifts of up to  $10.4 \text{ cm}^{-1}$  (2,0) for the various observed transitions for the lightest and the heaviest isotopes. The experimental findings are in good agreement with these predictions.

The spectra scanned for AgCl at the two Ag mass channels differ slightly from those of the AgCl mass channels. The intensity pattern is changed, although the peak positions are in rather good agreement. The fact that the (2,0) transition is the most intense feature in the Ag detected AgCl MRES and the (0,0) transition is rather weak, gives a clear hint about the position of the intermediate dissociative potential curve through which the AgX neutral fragmentation occurs. The mass spectrum related to the features observed in Fig. 3 is quite interesting and revealing. Figure 4 shows the mass spectra of AgCl obtained by excitation at three different vibronic transitions of AgCl's  $B \leftarrow X$  system followed by subsequent dye laser ionization to generate  $\text{Ag}^+$  and by excimer laser ionization to generate  $\text{AgCl}^+$ . A number of points are worth noting concerning these TOFMS data.

First, the AgCl dissociates in the excitation/ionization

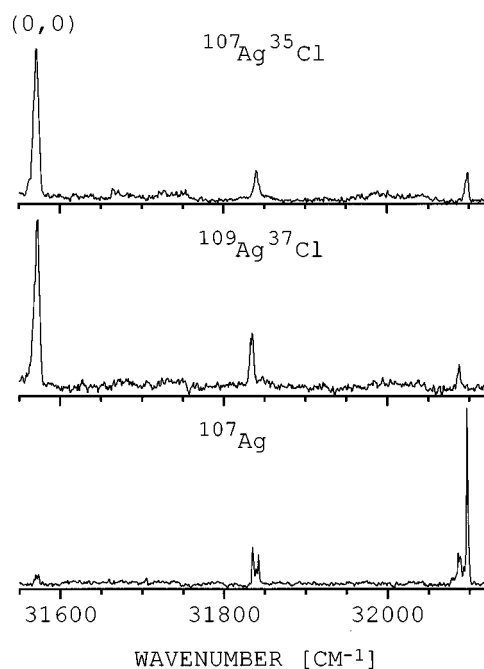


FIG. 3. Two-color MRES of AgCl. The spectra were recorded for dye laser excitation of the  $B \leftarrow X$  transition and ArF excimer laser ionization. The figure compares the spectra taken in the mass channels  $^{107}\text{Ag}^{35}\text{Cl}$  and  $^{109}\text{Ag}^{37}\text{Cl}$  with the spectrum from the  $^{107}\text{Ag}$  mass channel. The latter is the result of a one-color multiphoton ionization with only a dye laser under identical expansion conditions. These conditions generate  $\text{Ag}^*$  after the second photon is absorbed and  $\text{Ag}^+$  upon subsequent photon absorption by  $\text{Ag}^*$ . The intensity disparity for the (2,0) isotope features in the molecular isotopic mass channels mirrors directly the  $1:3 = ^{37}\text{Cl}:^{35}\text{Cl}$  abundance ratio. The intensity pattern for the  $^{107}\text{Ag}$  mass detected AgCl spectrum is explained in the text.

process, generated by the dye laser only. Dissociation takes place on the intermediate state surface (after the second of three photons is absorbed) because excimer laser (1+1) ionization does not yield  $\text{Ag}^+$ , because the ionization cross section depends critically on  $\sim 500 \text{ cm}^{-1}$  in the  $B \leftarrow X$  transition (see Fig. 3), and because the (1+2) two-color ionization process generated by the dye laser only would be near threshold with little excess energy left remaining in the AgCl ion to break the  $\text{AgCl}^+$  bond. Moreover, the covariance mapping technique<sup>12</sup> is employed to reveal possible relations between silver halide bare ions ( $\text{AgX}^+$ ) and  $\text{Ag}^+$ . The measured normalized covariances and correlation coefficients between  $\text{AgCl}^+$  and  $\text{Ag}^+$  are zero (no correlation) for all possible isotopic combinations. Consequently, the formation of the  $\text{AgCl}^+$  and  $\text{Ag}^+$  ions must be independent.

Second, the expected mass peak widths are 20.6 ns for  $\text{Ag}^+$  and 24.0 ns for  $\text{AgCl}^+$ . The measured widths are, however, 46 and 76 ns, respectively. The  $\text{Ag}^+$  peak splitting can be attributed to fragmentation of AgCl at the intermediate state with release of 0.6 eV kinetic energy for (2,0) excitation, but the AgCl peak widths are caused by an unknown phenomenon. Laser polarization (parallel and perpendicular to the flight tube axis) changes the splittings of the  $^{107}\text{Ag}$  and  $^{109}\text{Ag}$  isotope features due to projection of the dissociation velocity of the Ag atom on the flight tube axis, but does not affect the AgCl peaks.

Third, one can tune the  $B \leftarrow X$  transition at higher vibra-

TABLE I. Observed transitions  $B \leftarrow X$  transitions in AgCl;  $\nu'$  = excited-state vibrational levels,  $\nu''$  = ground-state vibrational levels (in  $\text{cm}^{-1}$ ).

	$\nu''=0$	1	2	3	4	5	6	Isotope
$\nu'=0$	31 572.2 <sup>a</sup>	31 233.5	30 895.6					<sup>107</sup> Ag <sup>35</sup> Cl
	31 572.0 <sup>a</sup>	31 241.3	30 909.4					<sup>107</sup> Ag <sup>37</sup> Cl
	31 572.2 <sup>a</sup>							<sup>109</sup> Ag <sup>37</sup> Cl
1	31 835.4 <sup>a</sup>							<sup>109</sup> Ag <sup>37</sup> Cl
				30 827.8				<sup>109</sup> Ag <sup>35</sup> Cl
	31 841.8 <sup>a</sup>	31 501.9	31 163.7	30 829.5				<sup>107</sup> Ag <sup>35</sup> Cl
2	31 837.3		31 172.6					<sup>107</sup> Ag <sup>37</sup> Cl
	32 087.9 <sup>a</sup>							<sup>109</sup> Ag <sup>37</sup> Cl
	32 088.0 <sup>a</sup>				30 749.7			<sup>107</sup> Ag <sup>37</sup> Cl
	32 098.8 <sup>a</sup>	31 758.0	31 419.6	31 084.2	30 751.2			<sup>107</sup> Ag <sup>35</sup> Cl
	32 097.7 <sup>a</sup>			31 095.1				<sup>109</sup> Ag <sup>35</sup> Cl
3	32 341.6	32 001.1	31 663.1	31 326.0	30 993.1	30 660.0	30 335.0	Ag <sup>35</sup> Cl <sup>b</sup>
	32 328.3	31 995.1			31 006.5			Ag <sup>37</sup> Cl <sup>b</sup>
4		32 227.6	31 889.1					Ag <sup>35</sup> Cl <sup>b</sup>
		32 218.0	31 886.3					Ag <sup>37</sup> Cl <sup>b</sup>

<sup>a</sup>Obtained from mass resolved excitation spectra.<sup>b</sup>Silver isotopes not resolved.

tional modes so as to generate only one of the isotopes in the mass spectrum. This occurs because the isotope spectral features are better resolved as the excitation energy increases within the  $B$  state [see Figs. 3 or 4(c), for example].

Table II contains the molecular parameters for both the  $X$  and  $B$  states of AgCl. The AgCl (2,0) transitions detected in mass channels <sup>107</sup>Ag and <sup>109</sup>Ag show the contribution of

two species containing each particular isotope: <sup>107</sup>Ag <sup>35</sup>Cl/<sup>107</sup>Ag <sup>37</sup>Cl and <sup>109</sup>Ag <sup>35</sup>Cl/<sup>109</sup>Ag <sup>37</sup>Cl.

### C. Silver bromide

The FE spectrum of AgBr is similar to that of AgCl, as shown in the lower trace of Fig. 2. The spectrum is dominated by intense transitions arising from the zero-point level of the  $X$  state. Hot band transitions are visible, as well. These latter features can be suppressed completely by using a small nozzle hole diameter and carrier gas pressures of up to 30 psig for the expansion. As seen in Fig. 5, the spectra obtained for scans of selected AgBr mass channels appear sharp and with almost the same intensity distribution as found in the fluorescence excitation spectra. Again, the presence of silver and bromine isotopes causes a spectral shift that is well pronounced between the lightest and heaviest species. Table III tabulates these results. In contrast to the findings for AgCl, the (0,0) transition dominates the AgBr spectrum recorded at the silver monomer mass channel. The AgBr spectrum detected in the <sup>107</sup>Ag mass channel has both broad [(0,0), (1,0)] and sharp [(2,0)] features and intense [(0,0), (2,0)] and weak [(1,0), (3,0), (4,0),...] features as shown in Fig. 5. These differences suggest a number of excited intermediate states could be involved in the Ag\* dissociation with different lifetimes and different Franck-Condon factors. The spectra recorded in the silver mass channels show transitions previously observed for the <sup>107</sup>Ag and <sup>109</sup>Ag containing AgBr species. Explicitly: <sup>107</sup>Ag <sup>79,81</sup>Br at 31 245.0  $\text{cm}^{-1}$  (0,0), 31 417.5  $\text{cm}^{-1}$  (1,0), 31 582.8  $\text{cm}^{-1}$  (2,0), 31 738.7 and 31 735.2  $\text{cm}^{-1}$  (3,0), 31 876.4 and 31 879.6  $\text{cm}^{-1}$  (4,0), 32 001.0  $\text{cm}^{-1}$  (5,0); and <sup>109</sup>Ag <sup>79,81</sup>Br at 31 245.0  $\text{cm}^{-1}$  (0,0), 31 417.5  $\text{cm}^{-1}$  (1,0), 31 582.6  $\text{cm}^{-1}$  (2,0), 31 735.2 and 31 733.8  $\text{cm}^{-1}$  (3,0), 31 876.3 and 31 873.7  $\text{cm}^{-1}$  (4,0), 31 998.3 and 32 001.3  $\text{cm}^{-1}$  (5,0). The molecular parameters for the surfaces  $B$  and  $X$  are given in Table II.

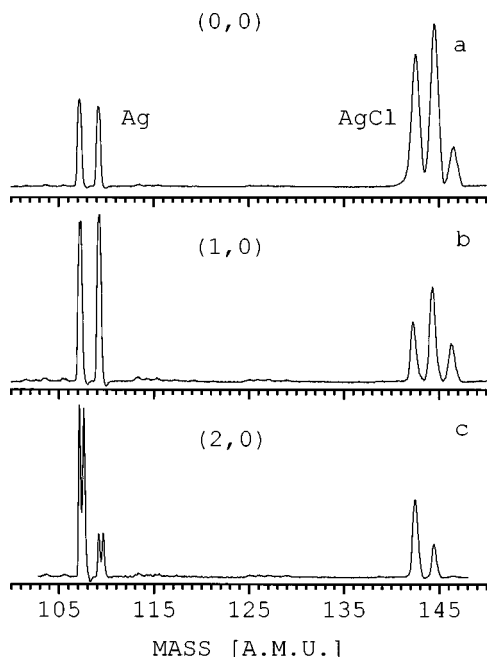


FIG. 4. Excitation energy dependent two-color MS of AgCl. The spectra were obtained by tuning the excitation laser to (a)  $\nu_{\text{exc}}=31\,583\text{ cm}^{-1}$  ( $\sim 0,0$ ), (b)  $\nu_{\text{exc}}=31\,844\text{ cm}^{-1}$  ( $\sim 1,0$ ), and (c)  $\nu_{\text{exc}}=32\,108\text{ cm}^{-1}$  ( $\sim 2,0$ ). Both the ArF excimer laser and the dye laser irradiate the molecular beam in this experiment. AgCl signals are obtained by excimer laser (1+1) two-color ionization and the Ag signals are obtained by (1+2) one-color ionization from the dye laser only. AgCl fragmentation occurs in the neutral molecule at  $\sim 64\,000\text{ cm}^{-1}$  to generate an excited Ag that is ionized by another dye laser photon. The third isotope feature at 146 amu is missing due to laser tuning (c).

TABLE II. Molecular constants of AgCl, AgBr, and AgI calculated based on Eq. (1); in  $\text{cm}^{-1}$ .

	$^{107}\text{Ag } ^{35}\text{Cl}$ $B \leftarrow X$		$^{109}\text{Ag } ^{81}\text{Br}$ $B \leftarrow X$		$^{107}\text{AgI}$ $B \leftarrow X$	
	This work	Brice <sup>a</sup>	This work	Brice <sup>a</sup>	This work	Brice <sup>a</sup>
$\nu_e$	31 604.73	31 606.92	31 277.14	31 280.43	31 197.45	31 190.87
$\omega_e'$	279.25	281.00	179.77	180.80	124.46	131.30
$\omega_e'x_e'$	4.3703	6.0	2.058	4.45	3.4611	5.175
$\omega_e'y_e'$	-0.3420	-0.095	-0.4515	-0.06	0.2126	-0.05
$\omega_e'z_e'$			-0.000 44		-0.081 96	
$\omega_e''^a$	343.60		247.72		206.18	
$\omega_e''x_e''^a$	1.163		0.679		0.433	
$\sigma^b$	0.214		0.219		0.080	
$\Delta\nu^c$	0.9		1.2		0.5	

<sup>a</sup>The ground state and comparison data are from Ref. 9.

<sup>b</sup>Standard deviation of the fit.

<sup>c</sup>Maximum deviation between the experimental and the fit peak positions (in  $\text{cm}^{-1}$ ).

## D. Silver iodide

Figure 6 shows the FE spectrum of the AgI  $B \leftarrow X$  transition and Fig. 7 shows mass resolved excitation spectra of AgI ( $B \leftarrow X$ ) detected in the mass channels of  $^{107}\text{AgI}$ ,  $^{109}\text{AgI}$ , and  $^{107}\text{Ag}$ . The  $B \leftarrow X$  (0,0) transition is no longer the most intense band in this spectrum, consistent with a slightly shifted excited state  $B$  potential surface with respect to the ground-state surface. An additional set of transitions ( $B' \leftarrow X$ ) is also observed in this region.

Figure 7(c) shows the mass resolved excitation spectrum of AgI as detected in the  $^{107}\text{Ag}$  mass channel. As can be seen, the spectrum includes all the transitions observed for the AgI isotopes, however the first four transitions of the  $B \leftarrow X$  transition are very weak as detected for a (1+2) one-

color dye laser only ionization scheme. The noteworthy change in signal intensities of certain peaks occurs because the intermediate state<sup>18</sup> ( $\sim 65\,000\text{ cm}^{-1}$ ) reached by the second photon is only weakly dissociative, while the energy is sufficient for dissociation at the (4,0) and (5,0) transitions. The  $B'$  state levels must access a different intermediate state that is always consistently somewhat dissociative.

As can be seen in Figs. 6, 7(a) and 7(b) the spectrum of AgI in the  $B \leftarrow X$  region consists of two progressions. The first set of features between  $30\,740$  and  $31\,635\text{ cm}^{-1}$  belongs to the  $B \leftarrow X$  transition (see Table IV) and a second different transition ( $B' \leftarrow X$ ) is found in the spectral region  $31\,613$  to  $32\,600\text{ cm}^{-1}$ . Based on vibrational spacing considerations, the feature observed at about  $31\,635\text{ cm}^{-1}$  might be an overlap of transitions that belong to both progressions.

The 3.8–4.1 eV region of the excited electronic manifold of AgI has been discussed by Mulliken,<sup>18</sup> Barrow,<sup>8</sup> Davidovits *et al.*<sup>5</sup> and Singh and Rai,<sup>19</sup> and it is extremely complicated and crowded with both bound and dissociative interacting zero-order potential-energy surfaces.

The  $B \leftarrow X$  absorption spectrum of silver iodide vapor in the near ultraviolet region has been observed and discussed by several groups.<sup>5–7,9</sup> In addition to the sharp  $B \leftarrow X$  features of AgI, a few very weak band heads on the top of a continuum in the region 300.0–320.0 nm are reported.<sup>9</sup> Since these weak features could not be fit into the vibrational analysis of the main progression, these transitions have remained unclassified.

Our jet experiments reproduce most of these less intense, unassigned features. In fact, due to both the cooling of AgI and the MRES technique, an entirely new progression of 27 well-resolved transitions is revealed (see Table V). For both sets of transitions, the vibrational isotope effect is detected, although it appears much more pronounced for the second progression. The  $B$  state exhibits its known strongly anharmonic shape with only a few vibrational levels which converge rapidly. Surprisingly, the newly discovered series of  $B'$  transitions shows a completely different vibrational behavior; the levels diverge slowly with a remarkably small vibrational energy.

Below we analyze two different possible explanations

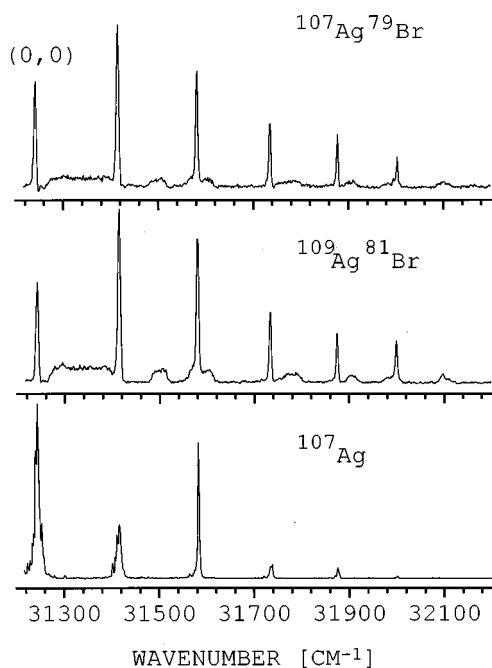


FIG. 5. MRES of AgBr recorded for the  $B \leftarrow X$  transitions in the AgBr and Ag mass channels. Spectra recorded in the AgBr mass channels 186 and 190 arise by two-color (1+1) dye plus excimer laser ionization and the spectrum recorded in the Ag mass channel arises by (1+2) one-color dye laser ionization.

TABLE III. Observed transitions  $B \leftarrow X$  transitions in AgBr;  $\nu'$ =excited-state vibrational levels,  $\nu''$ =ground-state vibrational levels (in  $\text{cm}^{-1}$ ).

	$\nu''=0$	1	2	3	4	6	Isotope
$\nu'=0$	31 243.0 <sup>a</sup>	30 996.8	30 751.3	30 508.3	30 262.7		<sup>107</sup> Ag <sup>79</sup> Br
	31 243.0 <sup>a</sup>						<sup>109</sup> Ag <sup>81</sup> Br
1	31 416.7 <sup>a</sup>	31 383.4	30 922.9	30 677.0			<sup>107</sup> Ag <sup>79</sup> Br
	31 415.3 <sup>a</sup>						<sup>109</sup> Ag <sup>81</sup> Br
2	31 582.8 <sup>a</sup>	31 333.3	31 086.2	30 849.8	30 596.0		<sup>107</sup> Ag <sup>79</sup> Br
	31 580.8 <sup>a</sup>						<sup>109</sup> Ag <sup>81</sup> Br
3	31 736.8 <sup>a</sup>	31 486.9				32 278.3	<sup>107</sup> Ag <sup>79</sup> Br
	31 734.1 <sup>a</sup>						<sup>109</sup> Ag <sup>81</sup> Br
4	31 878.6 <sup>a</sup>	31 624.2		31 135.5	30 895.5		<sup>107</sup> Ag <sup>79</sup> Br
	31 875.2 <sup>a</sup>						<sup>109</sup> Ag <sup>81</sup> Br
5	32 003.4 <sup>a</sup>						<sup>107</sup> Ag <sup>79</sup> Br
	31 999.8 <sup>a</sup>						<sup>109</sup> Ag <sup>81</sup> Br
6	32 099.9 <sup>a</sup>						<sup>109</sup> Ag <sup>81</sup> Br

<sup>a</sup>Obtained from mass resolved excitation spectra.

for the newly observed  $B'$  progression: 1. the  $B$  and  $B'$  progressions originate from two different electronic excited states; and 2. both progressions belong to one electronic state with a complicated single adiabatic potential surface. An example of a single potential yielding converging vibrational spacing for the first few vibrational levels followed by diverging spacing for the high vibrational levels is a so-called shelf state observed in alkali dimers. Those surfaces arise from avoided crossing between two diabatic potential surfaces.<sup>20</sup>

### 1. Two different electronic states

A possible and straight-forward assignment for the high-energy progression labeled  $B' \leftarrow X$  is that the transition terminates on a new bound electronic surface  $B'$  that is accessed from the ground potential surface. This new surface does not necessarily cross the  $B$  surface in the accessed Franck-Condon regions of  $B$  and  $B'$ ; they probably approach each other closely. The reasons for this assignment are as follows: (1) The  $B' \leftarrow X$  progression begins before the  $B \leftarrow X$  one ends; (2) although the progressions appear to be independent, a significant perturbation of the  $B'$  state, in the energy region in which both transitions exist, is apparent; (3) the  $B \leftarrow X$  progression abruptly ends at (5,0); (4) the  $B' \leftarrow X$

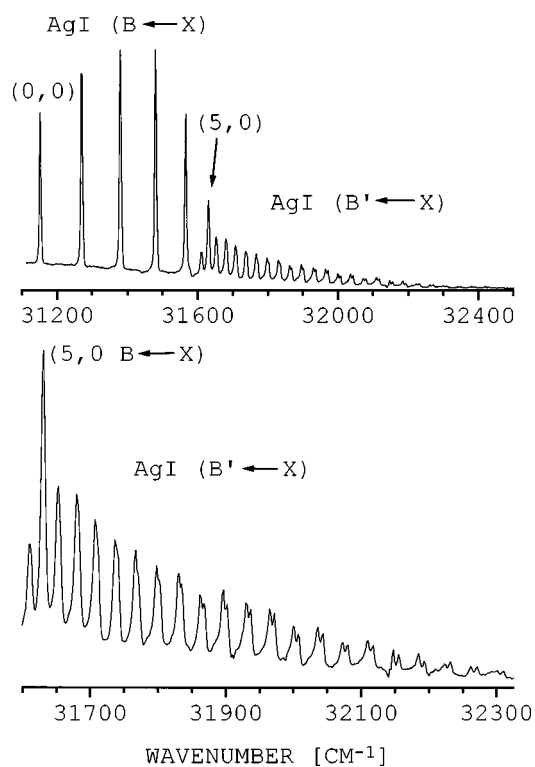


FIG. 6. FE spectra of expansion cooled AgI. The spectrum consists of two merged but distinguishable sets of progressions, the  $B \leftarrow X$  and  $B' \leftarrow X$  transitions. The previously unassigned  $B' \leftarrow X$  set shows a well-pronounced isotopic displacement. These features are discussed in the text. An expanded view of this latter transition is shown at the bottom of the figure.

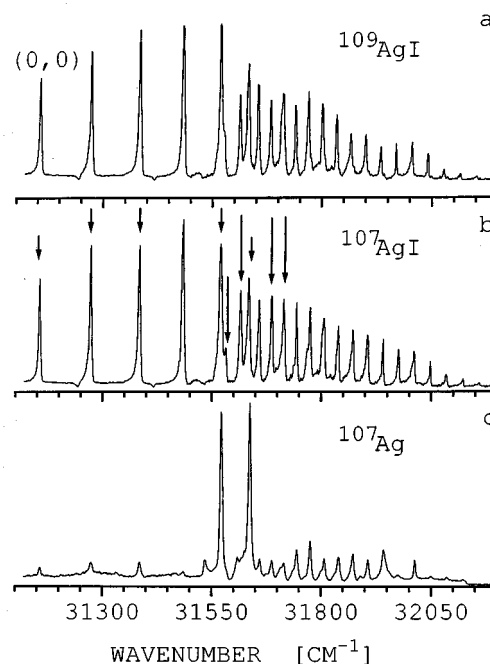


FIG. 7. (a) and (b) Two-color dye plus excimer laser MRES of AgI recorded for  $B \leftarrow X$  and  $B' \leftarrow X$  transitions in the mass channels <sup>109</sup>AgI, <sup>107</sup>AgI. The arrows associated with trace (b) are discussed in Fig. 10 caption. (c) One-color excitation spectrum of <sup>107</sup>AgI detected in the <sup>107</sup>Ag mass channel.

TABLE IV. Observed  $B \leftarrow X$  transitions in AgI;  $\nu'$  = excited-state vibrational levels,  $\nu''$  = ground-state vibrational levels (in  $\text{cm}^{-1}$ ).

	$\nu''=0$	1	2	3	4	5	Isotope
$\nu'=0$	31 156.0 <sup>a</sup>	30 946.2	30 743.5	30 538.0	30 338.4		<sup>107</sup> AgI
	31 156.0 <sup>a</sup>						<sup>109</sup> AgI
1	31 274.0 <sup>a</sup>	31 064.5	30 863.1		30 457.9	30 252.0	<sup>107</sup> AgI
	31 272.8 <sup>a</sup>						<sup>109</sup> AgI
2	31 384.3 <sup>a</sup>	31 175.2	30 971.0	30 763.0	30 563.0		<sup>107</sup> AgI
	31 383.6 <sup>a</sup>						<sup>109</sup> AgI
3	31 484.5 <sup>a</sup>				30 665.0		<sup>107</sup> AgI
	31 482.9 <sup>a</sup>						<sup>109</sup> AgI
4	31 570.3 <sup>a</sup>						<sup>107</sup> AgI
	31 570.2 <sup>a</sup>						<sup>109</sup> AgI
5	31 634.9 <sup>a</sup>						<sup>107</sup> AgI
	31 633.5 <sup>a</sup>						<sup>109</sup> AgI

<sup>a</sup>Obtained from mass resolved excitation spectra.

progression goes to a much higher energy than the  $B \leftarrow X$  progression ( $\sim 600 \text{ cm}^{-1}$ ) and thus they do not have a common dissociation limit; and (5) if the  $B$  surface were to have a second minimum and the  $B' \leftarrow X$  progression were associ-

ated with bound states contained in this second well, one would expect a very different Franck-Condon factor for  $B' \leftarrow X$  and a strong vibrational perturbation at the top of the barrier for this new minimum and at the dissociation limit.

TABLE V. Observed transitions for the  $B' \leftarrow X$  system of AgI (in  $\text{cm}^{-1}$ );  $\nu'$  = excited-state vibrational level,  $\nu''$  = ground-state vibrational levels. The  $B \leftarrow X$  transitions listed in Table IV comprise the first five transitions of the single surface analysis of the right hand side of the table. Also note that the (5,0) transition of Table IV is now labeled (6,0) for the single surface assignment for  $B, B' \leftarrow X$  on the right hand side of the present table. The <sup>107</sup>AgI molecule features are used for the fit to the isotopic data and the <sup>109</sup>AgI data are calculated to determine the isotope shift.

Measured transition energies $\nu_{\text{exp}}$		Transition assignments and the deviation between the calculated and the measured peak positions $\Delta\nu = \nu_{\text{calc}} - \nu_{\text{exp}}$							
		Two potential surfaces <sup>a</sup>		Single surface <sup>b</sup>		Modified single surface <sup>c</sup>			
<sup>109</sup> AgI	<sup>107</sup> AgI	$B' \leftarrow X$ ( $\nu', \nu''$ )	<sup>109</sup> AgI	<sup>107</sup> AgI	$B \leftarrow X$ ( $\nu', \nu''$ )	<sup>109</sup> AgI	<sup>107</sup> AgI	<sup>109</sup> AgI	<sup>107</sup> AgI
31 613.5	31 616.7	(0,0)	-0.42	-3.70	(5,0)	1.59	-0.86	5.02	2.03
31 633.5	31 634.9	(1,0)	2.03	0.29	(6,0)	2.18	1.35	-4.64	-4.88
31 655.3	31 659.0	(2,0)	4.27	0.37	(7,0)	1.79	-0.93	2.31	-0.49
31 683.7	31 687.6	(3,0)	1.69	-2.26	(8,0)	-0.02	-2.66	1.45	-1.15
31 710.7	31 715.2	(4,0)	2.10	-2.28	(9,0)	2.33	-0.69	3.76	0.68
31 739.8	31 744.6	(5,0)	1.84	-2.66	(10,0)	3.14	-0.07	2.76	-0.47
31 769.3	31 775.5	(6,0)	2.45	-3.26	(11,0)	3.15	-1.28	3.31	-1.06
31 801.0	31 806.8	(7,0)	1.99	-3.13	(12,0)	3.20	-0.50	3.78	0.04
31 834.1	31 839.3	(8,0)	1.12	-3.20	(13,0)	2.74	-0.26	2.60	-0.41
31 865.9	31 872.0	(9,0)	2.42	-2.59	(14,0)	3.12	-0.62	3.48	-0.23
31 899.5	31 906.0	(10,0)	2.69	-2.52	(15,0)	3.40	-0.42	3.49	-0.35
31 934.0	31 940.9	(11,0)	2.73	-2.67	(16,0)	3.34	-0.65	3.42	-0.55
31 969.0	31 975.7	(12,0)	2.85	-2.14	(17,0)	3.12	-0.50	3.34	-0.29
32 004.7	32 011.2	(13,0)	2.78	-1.80	(18,0)	3.14	-0.03	3.15	-0.01
32 040.6	32 047.6	(14,0)	2.96	-1.91	(19,0)	3.03	-0.38	3.23	-0.18
32 076.6	32 084.2	(15,0)	3.43	-1.82	(20,0)	3.55	-0.25	3.56	-0.25
32 114.0	32 122.6	(16,0)	2.87	-3.17	(21,0)	3.28	-1.23	3.38	-1.12
32 151.5	32 159.5	(17,0)	2.54	-2.69	(22,0)	3.81	0.12	3.88	0.19
32 188.8	32 198.3	(18,0)	2.74	-3.78	(23,0)	4.52	-0.51	4.54	-0.49
32 226.8	32 236.4	(19,0)	2.55	-3.84	(24,0)	4.42	-0.48	4.43	-0.47
32 265.5	32 275.1	(20,0)	1.99	-4.18	(25,0)	3.95	-0.75	3.97	-0.74
32 302.2	32 311.7	(21,0)	3.78	-2.05	(26,0)	5.44	1.01	5.35	0.90
32 341.0	32 351.1	(22,0)	3.86	-2.34	(27,0)	4.49	0.16	4.18	-0.17
32 381.0	32 390.3	(23,0)	3.16	-1.98	(28,0)	3.61	-0.02	3.11	-0.53
32 421.7	32 431.9	(24,0)	2.25	-3.53	(29,0)	2.48	-1.78	2.08	-2.14
32 462.1	32 472.3	(25,0)	2.19	-3.31	(30,0)	2.79	-1.01	2.69	-1.06
32 502.8	32 513.4	(26,0)	2.47	-3.13	(31,0)	3.70	-0.32	4.01	0.03
32 543.3	32 554.4	(27,0)	3.68	-2.11	(32,0)	4.69	0.31	5.09	0.69

<sup>a</sup>(0-20,0) obtained from MRES in the AgI mass channels; (21-27,0) obtained from FE spectra; the transition assignment is tentatively chosen.<sup>b</sup>Single RKR surface fitted to both  $B \leftarrow X$  and  $B' \leftarrow X$  progressions simultaneously.<sup>c</sup>Modified RKR surface with a local minimum in the shelf region.

The nature of this surface is at present not clear and can only be determined by a complete and very extensive *ab initio* calculation.

A least-squares analysis, third-degree polynomial fit of the spectroscopic data including the isotopic displacement can be undertaken for both progressions independently based on Eq. (1). This procedure leads to an accurate potential curve for the *B* state. The *B'* data are much more difficult to deal with since the absolute numbering of the observed transitions is ambiguous. Therefore, as a first approximation, we assume the *B'* (0,0) transition is the one observed at 31 616.7 cm<sup>-1</sup> (for <sup>107</sup>AgI) and we apply the fitting procedure to the *B'* state using the spectroscopic data given in Table V. The calculated isotopic displacement for each transition deviates apparently in a systematic manner from the experimentally obtained values (see Table V). Such fits rapidly become better if one assigns the 31 616.7 cm<sup>-1</sup> observed transition to a higher vibronic *B'* state [e.g., (6,0)]. Although this leads to smaller standard deviation fits, the overall result is suspect because the computed system origin, vibrational frequency, and the anharmonicities have physically unreasonable values.

In some instances one can determine the absolute labeling and the (0,0) transition position for a spectrum if one assumes that the isotopic displacement for transitions close to (0,0) is very small and that it increases noticeably at higher vibrational levels. That is, the isotopic splitting is fit to determine the vibronic numbering and the absolute vibration numbers in the excited states are obtained from the fit. Here too the fit parameters are not physically meaningful (e.g.,  $\omega_e < 0$ ).

If we treat the <sup>107</sup>AgI (and <sup>109</sup>AgI) data independently we obtain fits with acceptable standard deviations; however, the prediction of the <sup>109</sup>AgI transitions based on the <sup>107</sup>AgI data (and vice versa) by applying the factor  $\beta$  [see Eq. (3)] fails. Since it is not possible to explore the nature of these experimentally observed deviations from regular behavior in full detail, we choose the transition numbering shown in Table V and determine for the molecular constants of the *B'* state  $\nu_e = 31\,705.69$  cm<sup>-1</sup>,  $\omega_e = 20.01$  cm<sup>-1</sup>,  $\omega_e x'_e = 1.149$  cm<sup>-1</sup>,  $\omega_e y'_e = -0.0364$  cm<sup>-1</sup>, and  $\omega_e z'_e = 0.0005$  cm<sup>-1</sup>.

## 2. One potential surface

Alternatively, consider that both *B* and *B'* progressions belong to one electronic state with a complicated potential surface arising from avoided crossings between two (or more) diabatic surfaces. To examine this possibility, the Rydberg–Klein–Rees (RKR) method<sup>21</sup> is employed to obtain the potential curve for this state from the measured vibrational energies. In the RKR approach, one obtains the left- and right-hand turning points  $r_{\min}$  and  $r_{\max}$  for ro-vibrational level  $(\nu, J)$  of a potential surface from the Klein *f* and *g* integrals

$$r_{\max} - r_{\min} = 2f = \left( \frac{\hbar}{\pi \mu c} \right)^{1/2} \times \int_{-1/2}^{\nu} [G_J(\nu) - G_J(x)]^{-1/2} dx, \quad (4)$$

$$\frac{r_{\max} - r_{\min}}{r_{\min} r_{\max}} = 2g = 4 \left( \frac{\pi \mu c}{\hbar} \right)^{1/2} \times \int_{-1/2}^{\nu} B_J(x) [G_J(\nu) - G_J(x)]^{-1/2} dx, \quad (5)$$

in which  $G_J(\nu)$  is the vibrational energy and

$$B_J(\nu) \equiv \frac{\partial E(\nu, J)}{\partial [J(J+1)]}$$

is the effective rotational constant. Equation (4) is used to calculate the distance  $r_{\max} - r_{\min}$  between the outer and the inner turning points for each vibrational level  $\nu$  of the new potential surface. The function values  $G_J(x)$  between the measured energy levels  $G_J(\nu)$  are obtained by a cubic spline interpolation. The measured vibrational energies of the <sup>107</sup>AgI isotope are used in the calculation. The effective rotational constants  $B_J(\nu)$  needed in Eq. (5) cannot be obtained from our experiment because our spectral resolution ( $\sim 0.5$  cm<sup>-1</sup>) is lower than what would be needed for resolving individual rotational transitions of AgI. Therefore, we resort to the following approximate procedure. A Morse potential curve is fit to the  $r_{\max} - r_{\min}$  values calculated from the RKR method for  $\nu = 0, 1$ , and 2. The vibrational eigenvalues of the obtained Morse potential are nearly identical with the measured vibrational energies  $G_J(\nu)$  for  $\nu = 0, 1$ , and 2. This indicates that the RKR potential curve may be very close to the Morse curve at energies below the vibrational level  $\nu = 2$ . The equilibrium internuclear distance for this Morse potential is derived from the known rotational constant  $B_e = 0.0407$  cm<sup>-1</sup> measured in Ref. 6. The repulsive branch from this fitted Morse curve is then employed to calculate the positions of the inner turning points  $r_{\min}$  for all measured vibrational levels  $\nu$ . This approach is justified since the repulsive branch even in complicated potential curves is generally smooth and often is approximated by an exponential form. The outer turning points  $r_{\max}$  are calculated by adding the  $r_{\max} - r_{\min}$  values calculated from the RKR method to the above values of  $r_{\min}$ . The resulting potential curve is shown in Fig. 8 which also shows the ground-state potential curve taken from Ref. 19. The *B* state curve fit to both *B* and *B'* progressions has a shelf region on its outer wall between 3.0 and 3.6 Å which makes the potential well unusually wide.

The vibrational eigenfunctions for this *B* state potential curve are calculated by solving the radial Schrödinger equation by the method of Numerov and Cooley using the INTENSITY computer code by Zemke and Stwalley.<sup>22</sup> The calculated *B/B'* and *X* state eigenfunctions are used to compute the Franck–Condon factors and transition dipole moments for the *B* ← *X* ( $\nu, 0$ ) transitions. Figures 9(a) and 9(b) compare the measured and the calculated spectral intensities. The calculated intensities show the right trend with strong ( $\nu, 0$ ) transitions for  $\nu \leq 4$  and a weaker ( $\nu, 0$ ) progression for  $\nu > 4$ . In the calculation, this weaker progression reaches a minimum

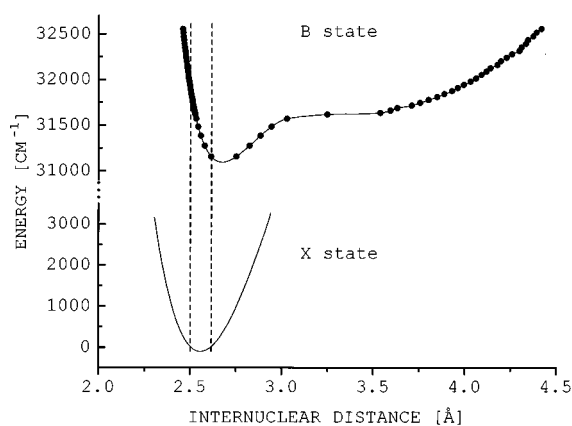


FIG. 8. Potential curve of AgI's  $B/B'$  state as obtained by RKR modeling of the observed  $^{109}\text{AgI}$  and  $^{107}\text{AgI}$  spectral data. This state has a well-pronounced shelf region between 3.0 and 3.6 Å. The ground-state potential curve data are taken from Ref. 19.

at  $\nu=6$  and a maximum at  $\nu=7$  or 8 while the experimental intensities reach a minimum at  $\nu=5$  and a maximum at  $\nu=6$ . Since the RKR method can only give two turning points, no local minimum can appear in the RKR potential curve. A better agreement with experimental intensities is achieved for a slightly modified  $B$  state RKR potential curve in the shelf region, with a local minimum well depth of about  $30\text{ cm}^{-1}$  at an internuclear distance of 3.42 Å. The calculated intensities for this modified RKR potential curve are shown in Fig. 9(c). The intensity minimum shifts to  $\nu=5$  and the

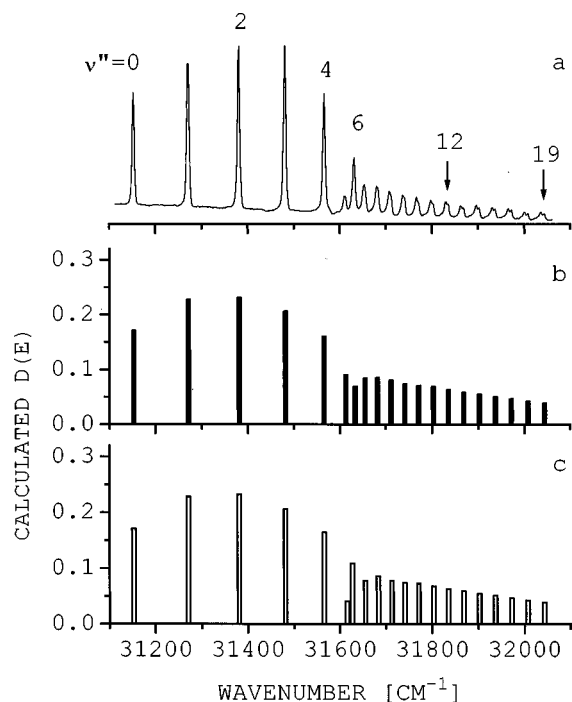


FIG. 9. (a) FE spectra of expansion cooled AgI, see caption of Fig. 6. (b) Calculated spectral intensities for the RKR potential curve (see Fig. 8). (c) Calculated spectral intensities for the modified RKR potential curve possessing a local minimum in the shelf region with well depth about  $30\text{ cm}^{-1}$  at internuclear distance 3.42 Å separated from the main well by a barrier at 3.20 Å.

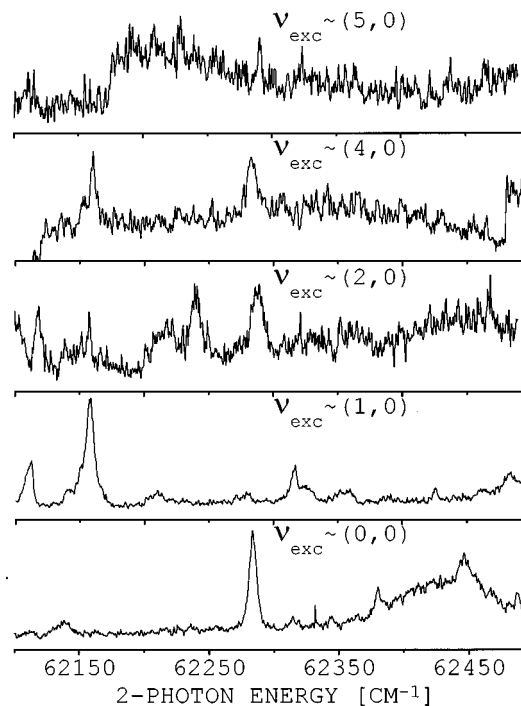


FIG. 10. Two-Color (1+2) dye laser MRES of AgI. The excitation laser is tuned to selected transitions of  $^{107}\text{AgI}$  of the  $B$  state; see short arrows in Fig. 7(b) for exact laser tuning positions.

weaker progression maximum occurs at  $\nu=6$  in better agreement with the experiment.

In both calculated spectra the intensities in the weaker progression decrease with increasing  $\nu$  somewhat slower than the experimental intensities. The calculated intensity decrease with  $\nu$  would be faster if the repulsive branch of the  $B$  state curve were less steep than that obtained from the Morse-curve extrapolation described above. Overall, the shelf state model (perhaps with a shallow local minimum in the shelf region) describes both the vibrational energies and the spectral intensities of the  $^{107}\text{AgI}$  isomer rather well. The only serious discrepancy with the experiment is for the isotopic displacement. Table V shows deviations between the calculated and the measured vibrational eigenvalues for both  $^{107}\text{AgI}$  and  $^{109}\text{AgI}$  isomers. Note that the deviation is small for  $^{107}\text{AgI}$  because its measured vibrational energies are employed to construct the RKR potential curve. The  $^{109}\text{AgI}$  eigenvalues calculated for this potential curve are larger than the measured ones. The calculated isotopic displacement is, therefore, systematically smaller than that experimentally observed—up to  $4\text{ cm}^{-1}$  smaller for  $\nu \leq 19$ .

Thus, we can fit the  $B \leftarrow X$  and  $B' \leftarrow X$  AgI spectrum (within the Born–Oppenheimer approximation) in two apparently reasonable ways: An RKR single electronic potential-energy surface; and two potential-energy surfaces for  $B$  and  $B'$  excited states. Nonetheless, neither gives a satisfactory model for what we know to be vibrational isotopic splitting.

### E. AgI—MRES of higher electronic states

The excited states of AgI have been the subject of numerous studies. The states located are the A [(0,0) at 23 879



- <sup>14</sup>J. A. Ternisien, *Metaux [Corrosion-Ind.]* **34**, 151 (1959).
- <sup>15</sup>K. Jellinek and A. Rudat, *Z. Phys. Chem. Abt. A* **143**, 55 (1929).
- <sup>16</sup>Gmelin Handbuch der anorganischen Chemie, Bd. 2-3 (Silver), Verlag Chemie GmbH, Weinheim/Bergstrasse (1970).
- <sup>17</sup>Huber and Herzberg, *Molecular Spectra and Molecular Structure, Vol. 1* (Krieger, Malabar, Florida, 1989).
- <sup>18</sup>R. S. Mulliken, *Phys. Rev.* **50**, 1017 (1936); **51**, 310 (1937); R. C. M. Learner, *Proc. Roy. Soc. [London] A* **269**, 327 (1962).
- <sup>19</sup>R. B. Singh and D. K. Rai, *Can. J. Phys.* **43**, 1685 (1965).
- <sup>20</sup>H. Wang, T.-J. Whang, A. M. Lyyra, L. Li, and W. C. Stwalley, *J. Chem. Phys.* **94**, 4756 (1991) and references therein.
- <sup>21</sup>W. C. Stwalley, *J. Chem. Phys.* **56**, 2485 (1972), and references therein.
- <sup>22</sup>W. T. Zemke and W. C. Stwalley, Program INTENSITY, Program No. QCPE477/QCMP171, Quantum Chemistry Program Exchange, Indiana University, Bloomington, Indiana.
- <sup>23</sup>N. Metropolis and G. Beutler, *Phys. Rev.* **55**, 1113 (1939).
- <sup>24</sup>R. F. Barrow and M. F. R. Mulcahy, *Nature (London)* **162**, 336 (1948).
- <sup>25</sup>N. Metropolis, *Phys. Rev.* **55**, 636 (1939).